Dalton Transactions

Accepted Manuscript

ROYAL SOCIETY OF CHEMISTRY

www.rsc.org/dalton

Journal Name

RSCPublishing

ARTICLE

The role of weak hydrogen and halogen bonding interactions in the assembly of a series of Hg(II) coordination polymers

Cite this: DOI: 10.1039/xoxxooooox

Alireza Azhdari Tehrani[a], Ali Morsali[a]* and Maciej Kubicki[b]

Received ooth January 2015,
Accepted ooth January 2015

DOI: 10.1039/xoxxooooox

www.rsc.org/

A series of eight new Hg(II) complexes based on the $L^{4\text{-}X}$ ligands, where L is (*E*)-4-halo-*N*-(pyridin-4-ylmethylene)aniline, synthesized, characterized and their supramolecular crystal structures were studied by different geometrical and theoretical methods. Our study reveals the role of weak intermolecular interactions involving halogens, such as C-H···X hydrogen bonds (in the cases of **1**, **2**, **3**, **5**, **6** and **7**) and C-X···X′-M halogen bonds (in the cases of **4** and **8**), in the structural changes of supramolecular assemblies of coordination compounds. Complexes **1**-**8** were also synthesized by sonochemical irradiation and the morphology of the prepared complexes was investigated using FE-SEM. The BFDH analysis helps us to compare the predicted morphology to that obtained under ultrasonication. This study may provide further insight into discovering the role of weak intermolecular interactions in the context of metallosupramolecular assembly.

Introduction

In the last two decades, crystal engineering of metal-containing compounds has received considerable attention due to their versatile structural diversity and widespread applications in diverse fields.[1] The bulk physical and chemical properties of molecular materials are intimately rooted to the relative orientation and organization of the constituent molecular building blocks. Therefore, it is evident that an ability to control this ordering would afford control over these properties.[2] In comparison to organic crystal engineering, the intricacies of metal-containing crystal packing are still not well understood due to the inherent complexities in predicting the structural outcome of the supramolecular architecture.[3] However, the final supramolecular architecture of self-assembled metal-containing compounds could be affected by different factors such as metal and ligand geometries,[4] counterions[5] and the reaction conditions.[6] Accordingly, in the recent years, many supramolecular chemists and crystal engineers have become involved in designing metal-containing systems, aiming at understanding the intermolecular interactions (synthons) holding the three-dimensional arrays of inorganic and organometallic building blocks. Among the intermolecular interactions, hydrogen and halogen bonds have attracted increasing interest due to their potential capabilities to the design and construction of molecular materials.[7] Halogen bonding (XB) is a non-covalent interaction that is in some ways analogous to hydrogen bonding (HB) and may be represented schematically by D···X-Y, in which X is the electrophilic halogen atom (XB donor), D is a donor of electron density (XB acceptor), and Y is a carbon, nitrogen or halogen atom.[8] In the context of metallosupramolecular assembly, most of the studies related to XB concerns the crystal packing analysis of metal-containing species with different halogen substituted ligands which are capable of halogen bonding.[9] The results of these studies provide insights into the recognition of different halogen bonding synthons, involving at least one inorganic component, that could be a potential supramolecular glue in the supramolecular construction of hybrid organic–inorganic systems.[10]

As part of our research program aimed at understanding the supramolecular features of mercury(II) coordination compounds,[11] a series of (*E*)-4-halo-*N*-(pyridin-4-ylmethylene)aniline ligands, $L^{4\text{-}F}$, $L^{4\text{-}Cl}$, $L^{4\text{-}Br}$ and $L^{4\text{-}I}$, in which the halogen atoms are in the phenyl *para*-position, have been used for the preparation of a series of mercury(II) complexes. Eight new mercury(II) coordination compounds, $[HgBr_2(L^{4\text{-}F})]$ (**1**), $[HgBr_2(L^{4\text{-}Cl})]$ (**2**), $[HgBr_2(L^{4\text{-}Br})_2]$ (**3**) and $[HgBr_2(L^{4\text{-}I})]$ (**4**), $[HgI_2(L^{4\text{-}F})]$ (**5**), $[HgI_2(L^{4\text{-}Cl})]$ (**6**), $[HgI_2(L^{4\text{-}Br})]$ (**7**) and $[HgI_2(L^{4\text{-}I})]$ (**8**) have been prepared by both conventional and sonochemical methods. The synthesized complexes were characterized and their crystal structures were determined. The crystal structure of these complexes was investigated by geometrical analysis, Hirshfeld surface analysis,[12] XPac analysis[13] and theoretical calculations. The study reveals that, in the cases of mercury(II) complexes with fluorinated, chlorinated and brominated ligand, the crystal packing is driven by C-H···X hydrogen bonding motifs, while in the cases of mercury(II) complexes with iodinated ligand, the C-X···X′-M halogen bonds play non-negligible role in the assembly of corresponding coordination polymers.

Results and Discussion

Synthesis

The ligands $L^{4\text{-}F}$, $L^{4\text{-}Cl}$, $L^{4\text{-}Br}$ and $L^{4\text{-}I}$ were synthesized by mixing the same equivalents of *para*-haloaniline and 4-pyridinecarboxaldehyde in ethanol. After stirring for 30 minutes at room temperature, the ligand precipitated from the reaction mixture as a yellow powder which was filtered and dried under vacuum. The reaction of equimolar quantities of $L^{4\text{-}X}$ ligands and HgX_2 (X=Br and I) in

methanol gave the corresponding Hg(II) complexes. The obtained complexes were insoluble in the reaction medium and were therefore they were recrystallized in hot acetonitrile. Single crystals of complexes **1**-**8** suitable for X-ray crystallography were obtained by slow evaporation of the solvent, after a few days. The crystallographic data, for compounds **1**-**8**, are listed in Table 1. Selected bond distances and angles are summarized in Table 2.

Structural analysis of $HgBr_2$ complexes, $[HgBr_2(L^{4-F})]$ (1), $[HgBr_2(L^{4-Cl})]$ (2), $[HgBr_2(L^{4-Br})_2]$ (3) and $[HgBr_2(L^{4-I})]$ (4)

X-ray crystallography analyses reveal that **1**, **2**, **3** and **4** crystallize in triclinic $P\bar{1}$, orthorhombic $P2_12_12_1$, orthorhombic $Fdd2$ and monoclinic $P2_1/c$ space groups, respectively. ORTEP diagrams of **1**-**8** drawn with 30% probability have been shown in Figure S1 (see supporting information).[14] The asymmetric unit of **1** contains two crystallographically independent Hg^{2+} ions, two coordinated 4-fluoro-*N*-(pyridine-4-ylmethylene)aniline (L^{4-F}) ligands and four bromide ions. The two crystallographically independent Hg(II) atoms have five-coordinate square pyramid coordination with the pyridine nitrogen atom of the L^{4-F} ligand in the axial position and four bridging bromide ions forming the equatorial plane, Figure S1. Selected bond distances and angles are listed in Table 2. The indices of trigonality,[15] as proposed by Addison and Reedijk, which lie in between square pyramidal (τ_5=0) and trigonal bypyramidal (τ_5=1), are τ_5= 0.05 and 0.06 for **1** which implies that the coordination geometries are best descried as square-pyramids. Figure 1(a) depicts the structure of a section of the chain polymer of **1** extending along the *a*-direction. The interchain packing arrangement of this compound shows how discrete 1D coordination polymers are linked together via C-H···Br, C-H···N and $R_2^2(8)$ motifs of C-H···F hydrogen bonding interactions between the adjacent chains, leading to the overall crystal structures, Figure 1(b), Table S1. The intrachain Hg···Hg distance is 3.978(1) Å and the intrachain Hg···Hg···Hg angle is 180.0˚, which implies weak mercurophilic interactions.[16]

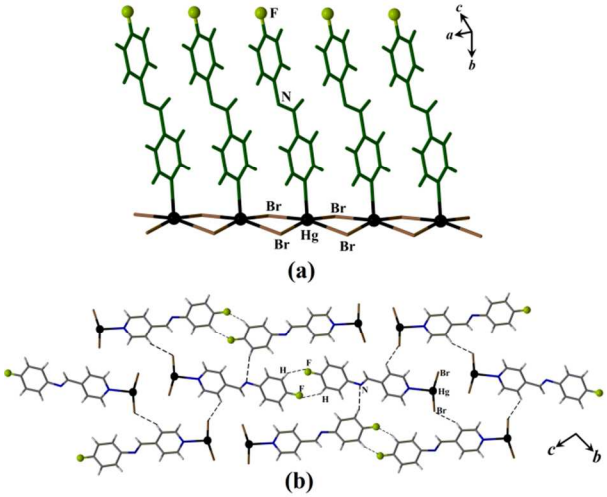

Figure 1. Representation of the 1D linear chain in **1** (a) a side view representation of **1,** showing the association of the adjacent chains through C-H···Br, C-H···N and $R_2^2(8)$ motifs of C-H···F hydrogen bonding interactions in the *bc*-plane (b).

The asymmetric unit of **2** consists of one Hg^{2+} ion, two bromides and one crystallographically independent L^{4-Cl} ligand. As depicted in Figure S1, according to the four-coordinate geometry index,[17] τ_4, proposed by Houser, the highly distorted tetrahedral geometry of the metal center can be described as a seesaw structure, with a τ_4 value of 0.71. The Br-Hg-Br angle is 158.64(3)˚, where the two Hg-Br bonds form the plank (Hg-Br1=2.4598(4) and Hg-Br2=2.4935(8) Å, Table 2). The angle between the other two bonds (Hg-N=2.397(6) Å and Hg-$Br2^i$=2.9913(9) Å (i):1/2+x, 2.5-y,1-z, Table 2) which form the pivot is 100.7(1)˚. The Br-Hg-Br and Br-Hg-N planes are nearly perpendicular with a dihedral angle of 89.92(1)˚. The $[HgBr(L^{4-Cl})]$ beads are threaded by the bromide bridge (Br2) to form a helical one-dimensional coordination polymer that propagates along a 2_1 screw axis in the *a*-direction. The helical 1D chain is further stabilized by a combination of weak intrachain Cl···π (Cl···ring-centroid= 3.425(4)Å) and N···π (N···ring-centroid= 3.436(7) Å) interactions, Figure 2(a) and Table S1. As shown in Figure 2(b), these 1D helical chains are further linked to each other by C-H···Br and C-H···Cl hydrogen bonding interactions.

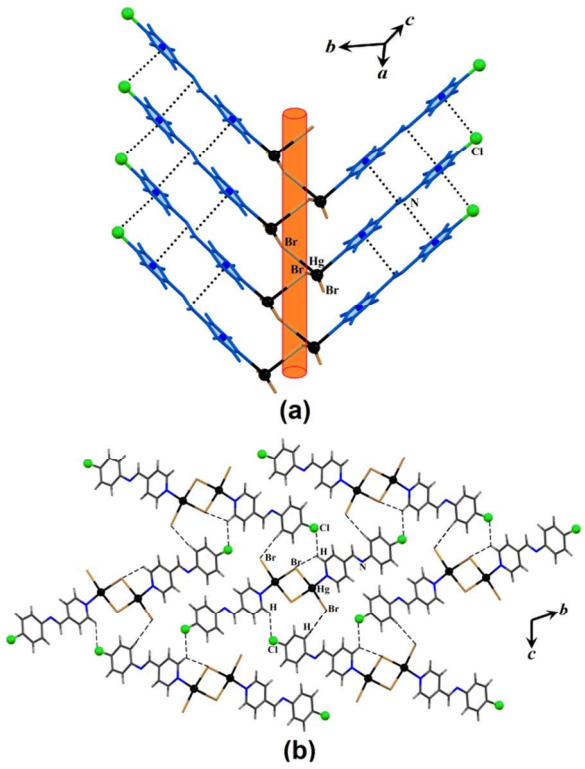

Figure 2. Representation of the helical one-dimensional coordination polymer in **2** (a) a side view representation of **2,** showing the association of the adjacent chains through C-H···Br and C-H···Cl hydrogen bonding interactions in the *bc*-plane (b).

There is one independent L^{4-Br} ligand, one bromide ion and half of the Hg(II) ion, which lies on the two-fold rotation axis, in the asymmetric unit of the crystal structure of **3**. The Hg(II) ion is four-coordinate in the seesaw geometry (τ_4=0.72), coordinated by two pyridine nitrogen atoms of the L^{4-Br} ligands (Hg-N=2.409(8) Å) and two bromide ions (Hg-Br=2.4974(11) Å). In the crystal structure of **3**, discrete neutral $[HgBr_2(L^{4-Br})_2]$ units stacked on one another in the *c*-direction by a combination of weak Br···π (Br···ring-centroid= 3.559(5) Å), N···π (N···ring-centroid= 3.436(10) Å) and C-H···Br interactions, Figure 3, Table S1.

Table 1. Structural data and refinement parameters for compounds **1-8**.

	1	**2**	**3**	**4**	**5**	**6**	**7**	**8**
formula	$C_{12}H_9Br_2FHg\ N_2$	$C_{12}H_9Br_2ClHgN_2$	$C_{24}H_{18}Br_4HgN_4$	$C_{12}H_9Br_2HgIN_2$	$C_{12}H_9FHgI_2N_2$	$C_{12}H_9ClHgI_2N_2$	$C_{12}H_9BrHgI_2N_2$	$C_{12}H_9HgI_3N_2$
fw	560.62	577.07	882.65	668.52	654.60	671.05	715.51	762.50
λ/Å	0.71073	0.71073	0.71073	0.71073	0.71073	0.71073	0.71073	0.71073
T/K	100	100	100	100	100	100	100	100
crystal system	Triclinic	Orthorhombic	Orthorhombic	Monoclinic	Orthorhombic	Orthorhombic	Orthorhombic	Monoclinic
space group	$P\bar{1}$	$P2_12_12_1$	$Fdd2$	$P2_1/c$	$Fdd2$	$P2_12_12_1$	$Pna2_1$	$P2_1/c$
a/Å	3.9779(2)	4.7120(2)	26.9001(7)	4.0584(2)	37.6061(3)	4.7590(2)	16.3554(7)	4.2727(2)
b/Å	18.8497(7)	16.4085(7)	37.9178(9)	23.4890(6)	38.3258(8)	16.9800(10)	22.6143(7)	24.0248(8)
c/Å	19.0199(8)	17.6773(8)	4.8030(2)	15.5548(5)	4.2956(2)	18.1555(7)	4.2385(2)	15.4948(5)
α/°	104.225(3)	90	90	90	90	90	90	90
β/°	91.415(3)	90	90	94.887(3)	90	90	90	95.495(3)
γ/°	94.296(3)	90	90	90	90	90	90	90
V/Å^3	1377.17(11)	1366.75(10)	4899.0(3)	1477.41(9)	6191.2(3)	1467.11(12)	1567.68(11)	1588.87(15)
D_{calc}/Mg.m^{-3}	2.714	2.804	2.393	3.006	2.809	3.038	3.032	3.199
Z	4	4	8	4	16	4	4	4
μ (mm^{-1})	16.972	17.285	12.830	17.900	13.928	14.865	16.290	15.556
F(000)	1016	1048	3280	1192	4640	1192	1264	1336
2θ (°)	50.00	51.99	56.30	50.00	51.98	49.99	56.51	50.00
R (int)	0.0499	0.0475	0.0611	0.0737	0.0677	0.1119	0.0356	0.0483
GOOF	1.260	1.034	1.125	1.204	1.024	0.977	0.940	1.356
R_1[a](I>2σ(I))	0.0750	0.0221	0.0369	0.0783	0.0251	0.0490	0.0296	0.0587
wR_2[b](I>2σ(I))	0.2198	0.0473	0.0891	0.2144	0.0584	0.1052	0.0454	0.1609
CCDC No.	1034446	1034447	1034448	1034449	1034450	1034451	1034452	1034453

[a] $R_1 = \Sigma||F_o| - |F_c||/\Sigma|F_o|$. [b] $wR_2 = [\Sigma(w(F_o^2 - F_c^2)^2)/\Sigma w(F_o^2)2]^{1/2}$

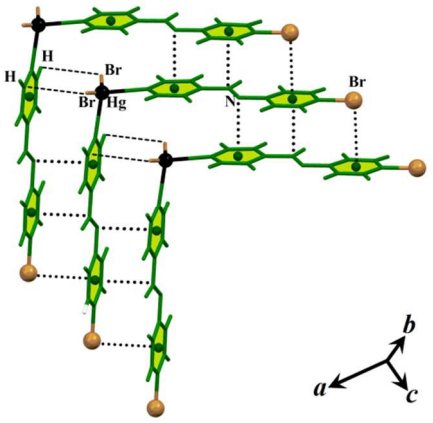

Figure 3. A side view representation of **3,** showing the stacking of the discrete units in the *c*-direction by a combination of weak Br···π, N···π and C-H···Br interactions.

Within the asymmetric unit of **4**, there is one Hg(II) ion, two bromide ions and one coordinated $L^{4\text{-}I}$ ligand. Metal atom is in the seesaw geometry, with a four coordinate geometry index, τ_4=0.79, coordinated by two Br ions (Hg-Br1=2.469(3) Å and Hg-Br2=2.464(3) Å, Table 2) at the plank and one pyridine nitrogen atom (Hg-N=2.38(2) Å) of the $L^{4\text{-}I}$ ligand and one bromide (Hg-Br1^i=3.154(3) Å, (i):-1+x, y, z), which form the pivot. The dihedral angle between the plane of Br-Hg-Br and N-Hg-Br is 88.35(2)°. In **4**, the 1D zigzag chain is generated from the μ_2 bridging mode of Br1, connecting each Hg center through a Hg-Br-Hg bridge in the *a*-direction, Figure 4(a). The intrachain Hg···Hg distance is 4.058(1) Å and the intrachain Hg···Hg···Hg angle is 180.0°. As shown in figure 4(b), the final supramolecular arrangement results from the linkage of neighboring coordination polymers through C-I···Br-Hg (C-I···Br=3.580(3)Å C-I···Br=173.0(7)°) halogen bonding and weak C-H···Br hydrogen bonding interactions, in the *bc*-plane, Table 3 and Table S1.

Structural analysis of HgI_2 complexes, $[HgI_2(L^{4\text{-}F})]$ (5), $[HgI_2(L^{4\text{-}Cl})]$ (6), $[HgI_2(L^{4\text{-}Br})]$ (7) and $[HgI_2(L^{4\text{-}I})]$ (8)

X-ray crystallography analyses reveal that **5**, **6**, **7** and **8** crystallize in orthorhombic $Fdd2$, orthorhombic $P2_12_12_1$, orthorhombic $Pna2_1$ and monoclinic $P2_1/c$ space groups, respectively. The asymmetric unit of all the compounds contain one crystallographic independent Hg^{2+} ion, two iodide ions and one $L^{4\text{-}X}$ (X=F, Cl, Br and I) ligand. In these

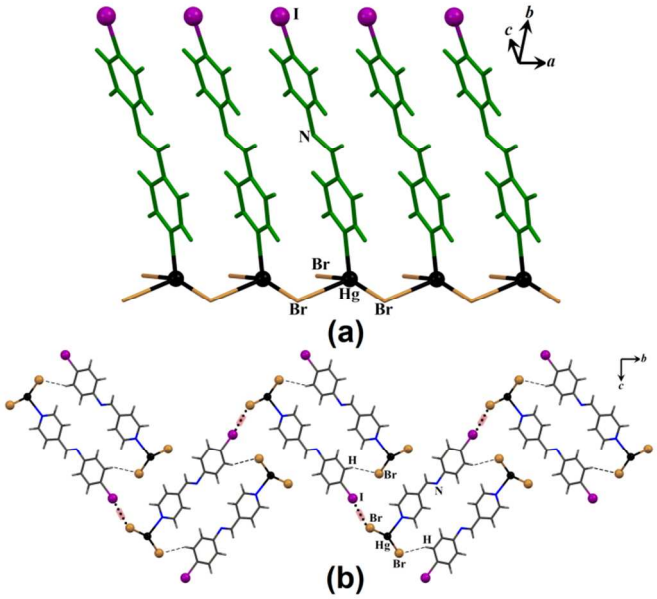

Figure 4. Representation of the one-dimensional coordination polymer in **4** (a) a side view representation of **4,** showing the association of the adjacent chains through C-I···Br-Hg halogen bonding and C-H···Br hydrogen bonding interactions in the *bc*-plane (b). Halogen bonds are highlighted in red.

structures, the coordination geometry around the Hg(II) can be described as a seesaw structure. The values of the geometrical index τ_4 of ca. 0.78, 0.68, 0.74 and 0.79 indicate the seesaw structure for the metal ion in the **5**, **6**, **7** and **8**, respectively. The seesaw coordination sphere around the Hg(II) atom is formed by two iodide ions as the plank and one iodide and one pyridine nitrogen atom in the pivot position, Figure S1. The dihedral angles between the I-Hg-I and N-Hg-I planes are 89.02(1), 89.23(4), 88.76(9) and 89.70(2)˚ for **5**, **6**, **7** and **8** respectively. Selected bond distances and angles are listed in Table 2.

7 and **8** are 1D coordination polymers built up from iodide-bridged Hg(II) edge-sharing highly distorted tetrahedra extending along the *c*-direction (for **7**) and *a*-direction (for **8**), Figures 5(a) and 6(a). The isostructurality of complexes **4** and **8** was investigated using XPac2.0.[13] The corresponding Xpac dissimilarity index (*X*) is 4.8 (3D similarity), calculated for a cluster comprising a kernel (central molecule) and 16 shell molecules (neighbors). XPac analysis also shows the 1D similarity between **5** and **7,** Figure S2. The Hg···Hg distances within the metal chains are 4.2956(2), 4.2385(2) and 4.2727(9) Å for **5**, **7** and **8**, respectively. These distances are completely out of the van der Waals limit (3.1 Å) for the mercurophilic interactions.[18] As shown in Figures 7(b) for **5**, 5(b) for **7** and 6(b) for **8**, these 1D chains are further linked to each other by C-H···I-Hg and C-H···X-C hydrogen bonding interactions, Table S1. In the case of **8**, the carbon-bound iodine atom is involved in two different C-I···I-Hg halogen bonds, namely C-I_{12}···I_1-Hg (C-I···I=3.697(1) Å, C-I···I=176.2(5)˚) and C-I_{12}···I_2-Hg (C-I···I=3.939(2) Å, C-I···I=96.1(5)˚) and weak C-H···I hydrogen bonds, Table 3 and Table S1. Thus, the overall supramolecular structure is constructed by linking 1D chains via a combination of halogen and hydrogen bonding interactions in the *bc*-plane, Figure 6(b).

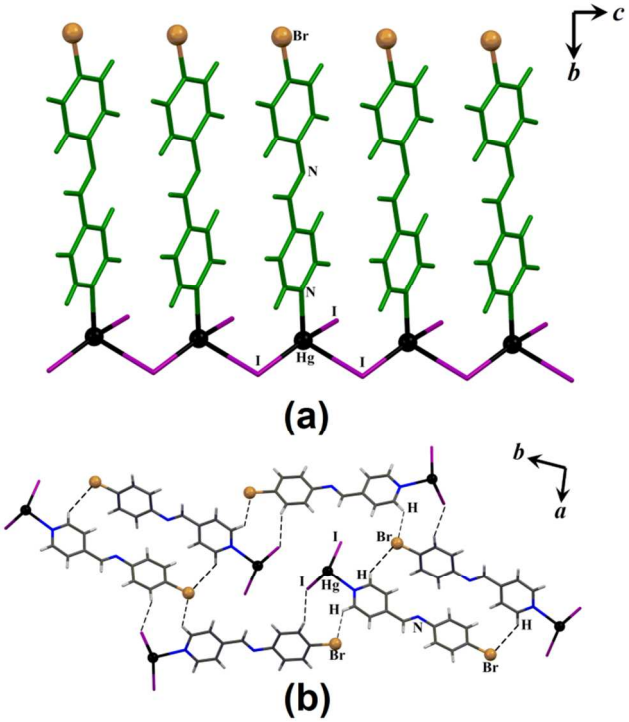

Figure 5. Representation of the one-dimensional coordination polymer in **7** (a) a side view representation of **7,** showing the association of the adjacent chains through C-H···I-Hg and C-H···Br-C hydrogen bonding interactions in the *ab*-plane (b).

The structure of **6** is isostructural with **2**. According to XPac analysis, these two complexes display 3D similarity (isostructurality) with the dissimilarity index of 2.9, Figure S2. The bridging of the iodide generates one-dimensional helical chain that propagates along a 2_1 screw axis parallel to the *a*-direction. An infinite helical mercury chain is further stabilized by a combination of weak intrachain Cl···π (Cl···ring-centroid= 3.475(7) Å) and N···π (N···ring-centroid= 3.342(15) Å) interactions, Figure 8(a). Adjacent 1D

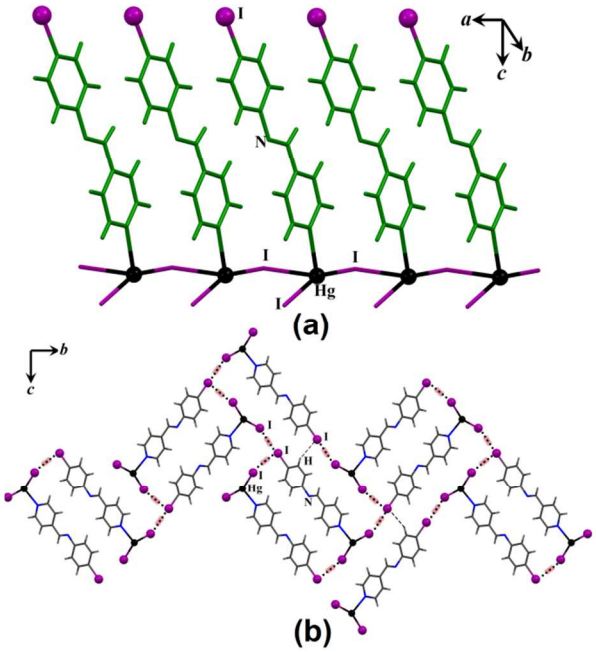

Figure 6. Representation of the one-dimensional coordination polymer in **8** (a) a side view representation of **8,** showing the association of the adjacent chains through C-I···I-Hg halogen bonding and C-H···I hydrogen bonding interactions in the *bc*-plane. Halogen bonds are highlighted in red (b).

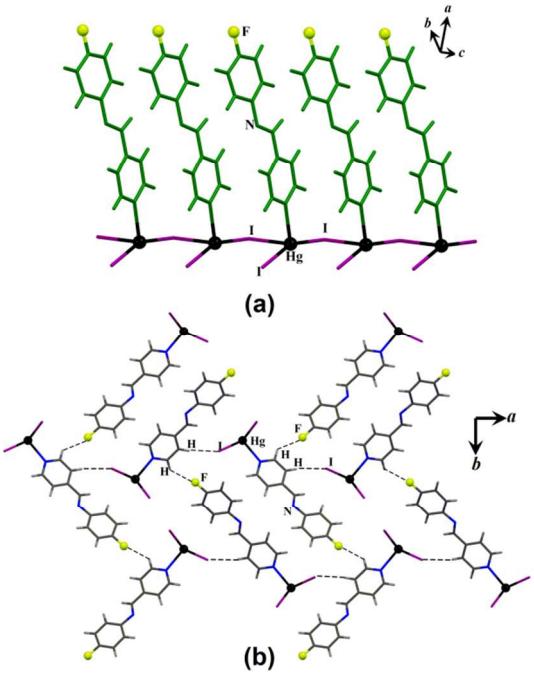

Figure 7. Representation of the one-dimensional coordination polymer in **5** (a) a side view representation of **5,** showing the association of the adjacent chains through C-H···I-Hg and C-H···F-C hydrogen bonding interactions in the *ab*-plane (b).

Table 2. Selected bond distances (Å) and angles (°) for complexes 1-8.

		Complex							
		1	**2**	**3**	**4**	**5**	**6**	**7**	**8**
Bond distance	Hg1-N1	2.43(2)	2.397(6)	2.409(8)	2.38(2)	2.424(7)	2.43(1)	2.431(9)	2.41 (1)
	Hg1-X1	2.478(2)	2.4598(8)	2.4974(11)	2.469(3)	2.625(1)	2.630(1)	2.642(1)	2.641(1)
	Hg1-X2	2.477(3)	2.4935(8)	-	2.464(3)	2.632(1)	2.650(1)	2.6571(8)	2.627(1)
	Hg2-N2	2.42(2)	-	-	-	-	-	-	-
	Hg2-X3	2.480(2)	-	-	-	-	-	-	-
	Hg2-X4	2.491(2)	-	-	-	-	-	-	-
Bond angle	N1-Hg1-X1	97.0(4)	101.7(1)	97.15(19)	100.6(5)	100.8(2)	102.2(3)	101.6(2)	102.6(3)
	N1-Hg1-X2	99.2(4)	96.2(1)	-	100.3(5)	102.9(2)	97.6(3)	97.6(2)	101.7(3)
	X1-Hg1-X2	163.70(9)	158.64(3)	-	156.41(9)	155.3(4)	156.00(4)	156.52(3)	155.57(4)
	N2-Hg2-X3	99.2(4)	-	-	-	-	-	-	-
	N2-Hg2-X4	96.1(4)	-	-	-	-	-	-	-
	X3-Hg2-X4	164.16(8)	-	-	-	-	-	-	-

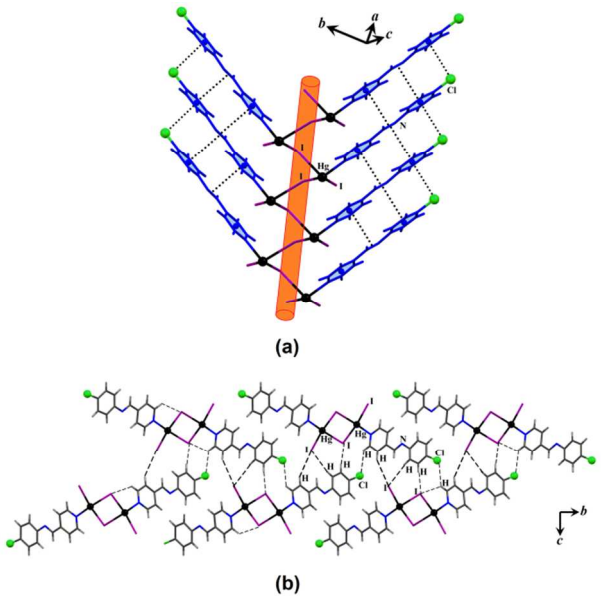

Figure 8. Representation of the helical one-dimensional coordination polymer in **6** (a) a side view representation of **6,** showing the association of the adjacent chains through C-H···I and C-H···Cl hydrogen bonding interactions in the *bc*-plane (b).

coordination polymers are further linked to each other by C-H···I and C-H···Cl hydrogen bonding interactions, Figure 8(b) and Table S1.

The role of weak hydrogen and halogen bonding interactions in the assembly of a series of Hg(II) coordination polymers

The ultimate aim of inorganic crystal engineering is the rational choice of intermolecular interactions to predict and design the assembly of metal-containing species. During the last two decades, much attention has been focused on understanding the role of intermolecular interactions in the context of metallosupramolecular chemistry.[19] A general strategy that has been used to identify this role is the systematic investigation of the crystal structures of closely related compounds.[20] Following this strategy, herein, the crystal structure study of a series of mercury(II) coordination compounds, based on the $L^{4\text{-}X}$ ligand (L= (*E*)-4-halo-*N*-(pyridin-4-ylmethylene)aniline) has been performed, in which the competition or cooperation between different types of non-covalent interactions involving halogens, namely weak hydrogen/halogen bonding interactions, is possible. It is to be noted that the d^{10} configuration of the Hg(II) ion is associated with a flexible coordination environment so that different geometries can be generated to tailor-make materials.[11d] A comparison between non-covalent interactions controlling the crystal packing of **1**-**8** is illustrated in Scheme 1. Except for **3**, crystal packing analysis reveals that 1D coordination polymers were obtained by the bridging ability of the halides. The coordination geometry of Hg(II), in **1**, is a distorted square-pyramid, while the coordination geometry around the metal center in complexes **2**-**8** is four-coordinated seesaw. In complexes **1** and **5**, where the Schiff base ligand $L^{4\text{-}F}$ is similar, different coordination geometry and structural motif is observed. These differences may be attributed to the halide ion size effect.[3d] Comparison between different types of non-covalent interactions in complexes **1**-**8** have been quantified via Hirshfeld surface analysis[12] and selected contribution percentages are shown as a histogram in Figure 9 and Table S2. The results of Hirshfeld surface analysis also revealed that the fluorine atom is mainly involved in interchain hydrogen bonding interactions of the type C-H···F. In the case of isostructural **2** and **6**, the chlorine atom is involved in weak intrachain Cl···π and interchain C-H···Cl hydrogen bonding interactions. The structural similarity of these two complexes also reflected in the similar contribution percentages of intermolecular interactions to the Hirshfeld surface area. The geometrical and Hirshfeld surface analyses of $[HgBr_2(L^{4\text{-}Br})_2]$,**3**, and $[HgI_2(L^{4\text{-}Br})]$,**7**, show that

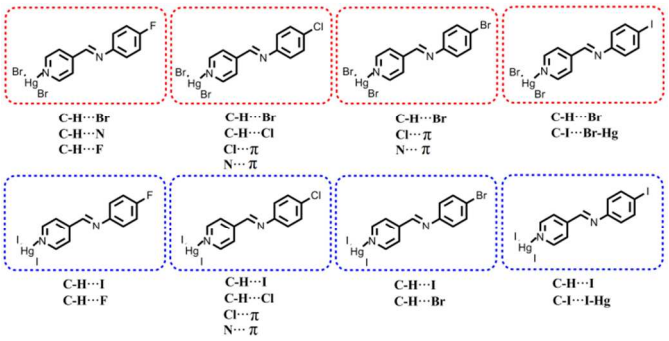

scheme 1. A comparison between non-covalent interactions controlling the crystal packing of complexes 1-8

Table 3. Halogen Bonding geometries and calculated XB binding energies for Compounds **4** and **8**

Complex	Interaction	C-I···X-Hg distance	C-I···X angle	Hg-X···I angle	Reduction of the sum of the VDW radii (%)	Symmetry code	Calculated interaction energy	Energy decomposition Analysis
[$HgBr_2(L^{4\text{-}I})$]	C_{12}-I_{12}…Br_1-Hg_1	3.580(3)	173.0(7)	110.89(4)	3.25	1-*x*,1/2+*y*,2.5-*z*	-11.61	ΔE_{Pauli}= 31.36 ΔE_{elstat}= -19.09 ΔE_{orb}= -11.77 ΔE_{disp}= -12.11
[$HgI_2(L^{4\text{-}I})$]	C_{12}-I_{12}…I_1-Hg_1	3.697(1)	176.2(5)	112.91(4)	6.65	2-*x*,-1/2+*y*,1.5-*z*	-7.17	ΔE_{Pauli}= 37.18 ΔE_{elstat}= -21.30 ΔE_{orb}= -13.89 ΔE_{disp}= -9.16
[$HgI_2(L^{4\text{-}I})$]	C_{12}-I_{12}…I_2-Hg_1	3.939(1)	96.1(5)	162.97(4)	0.54	3-*x*,-*y*,2-*z*	-2.44	ΔE_{Pauli}= 23.25 ΔE_{elstat}= -9.34 ΔE_{orb}= -6.66 ΔE_{disp}= -9.68

the bromine atom of the $L^{4\text{-}Br}$ ligand has the tendency to contribute in C-H···Br hydrogen bonding and Br··· π interactions in the self-assembly of discrete molecular complex **3** and coordination polymer **7**, respectively. The crystal structure analysis of the isostructural complexes **4** and **8** clearly revealed that the self-assembly is influenced by the C-X···X′-M halogen bonding interactions significantly. For **4** and **8,** the C-I···X′ distances of 3.580(3) and 3.697(1) Å are 3.25% and 6.65%, respectively, shorter than sum of the van der Waals radii, Table 3. The nearly linear angle of C-I···X′, 173.0(7)° for X′=Br and 176.2(5)° for X′=I, is in agreement with the concept of electron donation into the sigma antibonding orbital of C-X bond.[21] It is now well-established that the electron density is anisotropically distributed around the covalently bound halogen atoms.[22] Consequently, a region with a diminished electron density (σ-hole) is formed along the extension of the R-X bond. The magnitude of this region increases as the size and polarizability of the halogen atom increases, with a corresponding tendency for a halogen bond to become stronger.[23] Thus, not surprisingly, the iodine atom of the $L^{4\text{-}I}$ ligand has a greatest tendency to participate in halogen bonding interaction, as an electrophile. Also, it has been demonstrated that the organic (C-X) and inorganic (M-X′) halogens are serving different roles in C-X···X′-M halogen bonds, the former as an electrophile (XB donor) and the latter as a nucleophile (XB acceptor).[9c,9d,24] This can be understood by considering the alignment of the M-X group with the carbon bound iodine's σ-hole, Table 3. The halogen bonding interactions in **8**, in comparison to **4**, make up the greater contribution (I···Br=7.2% for **4** and I···I=11.2% for **8**), to the Hirshfeld surface area, Figure 9. The DFT calculation of the binding energy on two relative fragments of complex **4** and **8** clearly

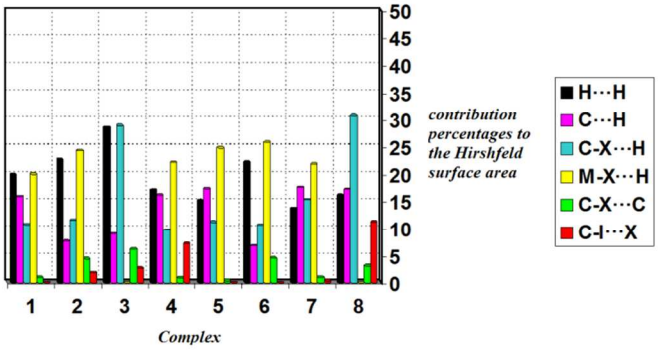

Figure 9. Relative contributions of various non-covalent contacts to the Hirshfeld surface area in complexes **1-8**.

show that the C-X···X′-M interaction binding energy decreases from **4** (-11.61 kJ/mol, symm. code: 1-*x*,1/2+*y*,2.5-*z*) to **8** (-7.17 kJ/mol, symm. code: 2-*x*,-1/2+*y*,1.5-*z*), Figure S3 and Table 3 (see computational details). Also, it should be noted that the value of the other halogen bonding energy in **8** (-2.44 kJ/mol, symm. code: 3-*x*,-*y*,2-*z*) is obtained when one of the monomers was rotated relative to the other by 180° while keeping the same I···I distance and C-I···I angle, Figure S3. Noteworthy, this interaction is less attractive since the angle requirement is not met and the $C\text{-}I_{12}\cdots I_2$ distance is close to or slightly below the sum of the van der Waals radii, Table 2 and Figure S4. To better insight into the nature of C-X···X′-M halogen bonds in **4** and **8**, energy decomposition analysis (EDA) at the BLYP-D3/TZ2P level of theory was applied. In the framework of Kohn-Sham molecular orbital theory, the total interaction energy can be decomposed into contributions of electrostatic interactions, orbital interactions, Pauli repulsion, and dispersion interaction. Table 3 provides the results of energy decomposition analysis for the halogen-bonded dimers in **4** and **8**. Noteworthy, the electrostatic term is the largest attractive term for C-I···X′-M (X′=Br and I) halogen bonding, which plays the most notable role in stabilizing the halogen-bonded dimers. This observation indicates that the electrostatic contribution is dominant over the charge-transfer contribution, since the lighter halide ion has more negative electrostatic potential.[25]

Sonochemical Synthesis of Complexes 1-8

It was interesting for us to evaluate the self-assembly of these complexes in the nano-scale realm. Correspondingly, complexes **1**-**8**, were readily synthesized by sonochemical method using an euqimolar amounts of $L^{4\text{-}X}$ (X=F, Cl, Br and I) ligands and $HgBr_2$ or HgI_2, in methanol, as starting materials at room temperature for 15 minutes (see experimental procedure). The products were characterized by different techniques such as powder X-ray diffraction (PXRD), IR spectroscopy and elemental analysis. The morphology and size of products prepared by the sonochemical method were examined by Field-Emission Scanning electron microscopy (FE-SEM), Figures 10 and S5. The SEM micrographs of complexes 1-8 show belt morphology for **1**, **3**, **5** and **7**, and rod morphology for **2**, **4**, **6** and **8** with diameters ranging from nano-to micro-dimensions. BFDH analysis was also carried out to estimate the faces that are likely to appear in the external morphology. This analysis considers the effect of symmetry operations on the interplanar distances of crystal faces.[26] Predicted crystal morphologies of complexes **1**-**8** are shown in Figures 10 and S5. In

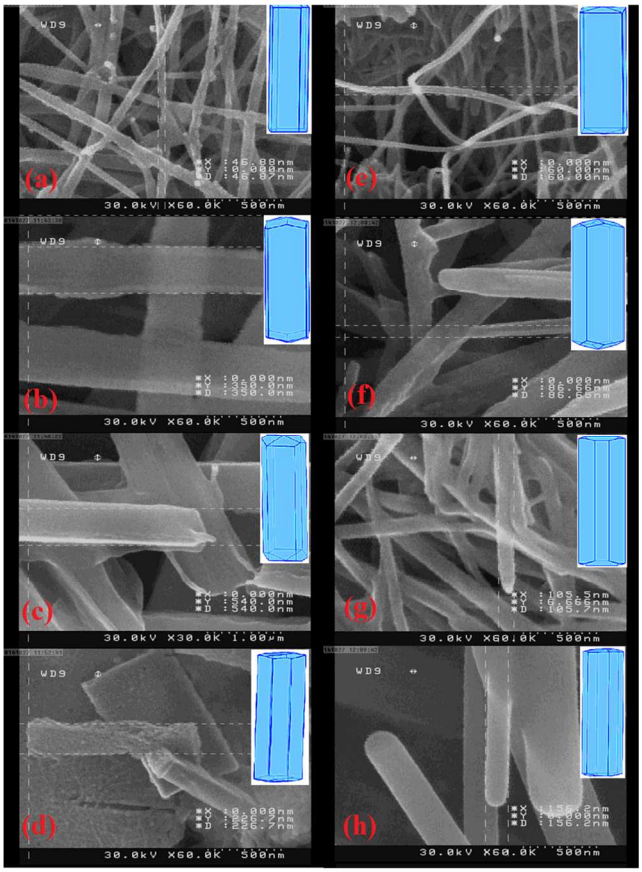

Figure 10. FE-SEM images of complexes **1-8** prepared by ultrasonic generator 305 Win. The right top inserts illustrate the predicted morphology of corresponding complexes **1**-**8**. **1** (a), **2** (b), **3** (c), **4** (d), **5** (e), **6** (f), **7** (g), **8** (h).

almost all cases there is a good match between the predicted morphology and observed habits. It should be noted that in the cases of **1**, **2**, **4**, **5**, **6**, **7** and **8**, the extension of the coordination polymer takes place along the [001], [011], [011], [220], [011], [110] and [011] directions, respectively, which are morphologically important and dominant in the crystal habit, Figure S6. Also, for **3**, the stacking of the discrete units via Br/N···π interactions occurs along the [220], thus (220) is the most important face. Details of the BFDH analysis are provided in the supporting information (Figure S6 and Table S3).

Conclusions

Eight new mercury(II) coordination compounds based on (*E*)-4-halo-*N*-(pyridin-4-ylmethylene)aniline (L^{4-X}) ligands were synthesized by conventional and sonochemical methods, characterized and their supramolecular structures were studied. An important feature of the synthesized complexes is the lack of strong hydrogen bond donor in the ligand skeleton, which means that these complexes could not self-assemble through strong hydrogen bonding interactions. As a result, in the closely related complexes **1**-**8**, weak intermolecular interactions, such as C-H···X hydrogen bonds (in the cases of **1**, **2**, **3**, **5**, **6** and **7**) and C-X···X′-M halogen bonds (in the cases of **4** and **8**), found the opportunity to direct the supramolecular self-assembly of the coordination compounds. The role of these weak intermolecular interactions involving halogens were investigated by geometrical analysis, Hirshfeld surface analysis, XPac analyses and theoretical calculations. Also, the synthesis of complexes **1**-**8** by the sonochemical method provides us an opportunity to investigate the self-assembly of these complexes in the nano-domain. The BFDH analyses were carried out to find the relationship between molecular aggregation and morphological features. We believe that it would be of interest to pursue studies such as these to clearly find out the missing ring between supramolecular chemistry and nanotechnology and to clarify the design of molecular materials with favorite morphology, size distribution and shape.

Experimental section

Apparatus and reagents

All starting materials and solvents were purchased from commercial suppliers (Sigma-Aldrich, Merck) and used as received. The infrared spectra were recorded on a Nicolet Fourier Transform IR, Nicolet 100 spectrometer in the range 500-4000 cm^{-1} using the KBr disk technique. Elemental analyses (carbon, hydrogen, and nitrogen) were performed using an ECS 4010 CHN-O made in Costech, Italy. Melting points were measured by a Electrothermal 9100 melting point apparatus and corrected. X-ray powder diffraction (XRPD) measurements were performed using a Philips Xpert diffractometer with monochromated Cu-Kα radiation (λ = 1.54056 Å). Ultrasonic generators were carried out on a SONICA-2200 EP, (maximum 305 W at 40 kHz). The samples were characterized by a field emission scanning electron microscope (FE-SEM) (Hitachi S-4160) with gold coating.

Single-Crystal Diffraction Studies.

X-ray diffraction data were collected at 100(1) K by the ω-scan technique on an Agilent Technologies four-circle diffractometer equipped with an Eos CCD-detector[27] using graphite-monochromatized Mo–Kα radiation (λ= 0.71073 Å). The data were corrected for Lorentz-polarization effects as well as for absorption.[27] Accurate unit-cell parameters were determined by a least-squares fit of reflections of the highest intensity, chosen from the whole experiment. The calculations were mainly performed within the WinGX program system.[28] The structures were solved with SIR92[29] and refined with the full-matrix least-squares procedure on F^2 by SHELXL97.[30] Non-hydrogen atoms were refined anisotropically, hydrogen atoms were placed in calculated positions and refined isotropically as riding with U_{iso} set at 1.2 times U_{eq} of the parent atom. Crystals of **4** and **5** appeared to be twinned, and this was taken into account in data reductions as well as in structure refinement. BASF factors (relative share of dominant component) were refined at 0.606(9) in **4** and 0.793(7) in **5**. In almost all cases (with exception of **3**, **4** and **5**) weak restraints (ISOR) were applied for lighter atoms to avoid eccentric shapes of some ellipsoids.

Computational Details.

DFT calculations were conducted by the ORCA quantum chemistry suite.[31] The BLYP exchange-correlation functional[32] with the recent D3 empirical dispersion correction[33] (BLYP-D3) was used to evaluate the binding energies. The basis set superposition error (BSSE) is not taken into consideration because small BSSE effects are assumed to be absorbed by the D3 empirical potential.[34] Decomposition of the interaction binding energy was also computed at BLYP-D3/TZ2P. The two selected fragments were cut out directly from the CIF data without optimization. An all-electron triple-zeta basis-set with two polarization functions, TZ2P, has been used to ascribe all the atoms. A frozen core approximation was used to treat the

core electrons. Scalar relativistic effects were account for by using the zeroth-order regular approximation (ZORA).[35]

Acknowledgements
The authors thank Tarbiat Modares University for all the supports. This research was supported by a grant (92024961) sponsored by the Iran National Science Foundation (INSF).

Notes and references
[a] Department of Chemistry, Faculty of Sciences, Tarbiat Modares University, P.O. Box 14115-175, Tehran, Iran
[b] Department of Chemistry, Adam Mickiewicz University, ul. Grunwaldzka 6, 60-780 Poznan, Poland

Electronic Supplementary Information (ESI) available: X-ray crystallographic files (CIF), Experimental details, ORTEP diagrams for complexes **1**-**8**, Selected fragments for halogen bonding energy analysis, BFDH details, and hydrogen bond parameters for complexes **1**-**8**. See DOI: 10.1039/b000000x/

References

(1) (a) S. Kitagawa, R. Kitaura, S. Noro, *Angew. Chem., Int. Ed*. 2004, 43, 2334-2375. (b) C. S. Liu, X. S. Shi, J. R. Li, J. J. Wang, X. H. Bu, *Cryst. Growth Des*. 2006, 6, 656-663. (c) S. G. Telfer, R. Kuroda, *Coord. Chem. Rev*. 2003, 242, 33-46. (d) S. A. Barnett, N. R. Champness, *Coord. Chem. Rev*. 2003, 246, 145-168. (e) C. D. Wu, A. G. Hu, L. Zhang, W. B. Lin, *J. Am. Chem. Soc*. 2005, 127, 8940-8941. (f) B. Moulton, M. J. Zaworotko, *Chem. Rev*. 2001, 101, 1629-1658. (g) M. Hong, *Cryst. Growth Des.*, 2007, *7*, 10–14. (h) E. R. T. Tiekink, J. Zukerman-Schpector, *CrystEngComm*, 2009, 11, 1176–1186 (i) K. Y. Wang, L. J. Zhou, M. L. Feng, X. Y. Huang, *Dalton Trans*., 2012, 6689-6695.
(2) (a) G. R. Desiraju, *Crystal Engineering. The Design of Organic Solids*; Elsevier: Amsterdam, 1989. (b) P. A. Gale, J. W. Steed, "Supramolecular Chemistry, from molecules to nanomaterials", John Wiley & Sons, Chichester, 2012. (c) G. R. Desiraju, *J. Am. Chem. Soc.*, 2013, *135*, 9952–9967 (d) G. R. Desiraju, *Angew. Chem. Int. Ed.* 2007, 46, 8342–8356. (e) S. Das, G. W. Brudvig, R. H. Crabtree, *Chem. Commun*., 2008, 413–424.
(3) (a) J. Reedijk, *Chem. Soc. Rev*., 2013, 42, 1776-1783 (b) E.C. Constable, *Chem. Soc. Rev*., 2007, 36, 246–253 (c) R. Chakrabarty, P. S. Mukherjee, P. J. Stang, *Chem. Rev*., 2011, 111, 6810–6918 (d) H. R. Khavasi, A. Azhdari Tehrani, *CrystEngComm*, 2013, 15, 5799-5812. (e) B. Cheng, A. Azhdari Tehrani, M-L. Hu, A. Morsali, *CrystEngComm*, 2014, 16, 9125–9134.
(4) (a) H. R. Khavasi, M. Mehdizadeh Barforoush, M. Azizpoor Fard, *CrystEngComm*, 2012, 14, 7236-7244 (b) A. Ovsyannikov, S. Ferlay, S. E. Solovieva, I. S. Antipin, A. I. Konovalov, N. Kyritsakas, M. W. Hosseini, *Inorg. Chem.*, 2013, 52, 6776 (c) H. R. Khavasi, M. Azizpoor Fard, *Cryst. Growth Des*., 2010, *10*, 1892–1896 (d) T. Hajiashrafi, A. Nemtai Kharat, J. A. Love, B. Patrick, *Polyhedron*, 2013, 60, 30-38.
(5) (a) B. L. Schottel, H. T. Chifotides, M. Shatruk, A. Chouai, L. M. Perez, J. Bacsa, K. R. Dunbar, *J. Am. Chem. Soc*., 2006, 128, 5895–5912. (b) L. Hashemi, A. Morsali, *New J. Chem.*, 2014, 38, 3187-3192. (c) V. Safarifard, A. Morsali, *CrystEngComm*, 2012, 14, 5130-5132. (d) G. Mahmoudi, A. Morsali, *CrystEngComm*, 2007, 9, 1062-1072. (e) F. Zeng, J. Ni, Q. Wang, Y. Ding, S. W. Ng, W. Zhu, Y. Xie, *Cryst. Growth Des*., 2010, 10, 1611–1622. (f) R. Custelcean, *Chem. Soc. Rev.*, 2014, 43, 1813-1824.
(6) (a) H. R. Khavasi, B. Mir Mohammad Sadegh, *Inorg. Chem.*, 2010, *49*, 5356–5358 (b) P. Mahata, M. Prabu, S. Natarajan, *Cryst. Growth Des.*, 2009, 9, 3683–3691. (c) S. T. Wu, L. S. Long, R. B. Huang, L. S. Zheng, *Cryst. Growth Des*., 2007, 7, 1746–1752.
(7) (a) A. Priimagi, G. Cavallo, G. Metrangolo, G. Resnati, *Acc. Chem. Res.*, 2013, *46*, 2686–2695. (b) A. V. Jentzsch, A. Hennig, J. Mareda, S. Matile, *Acc. Chem. Res.*, 2013, *46*, 2791–2800. (c) A. V. Jentzsch, S. Matile, *J. Am. Chem. Soc.*, 2013, *135*, 5302–5303. (d) J. de Groot, K. Gojdas, D. Unruh, T. Z. Forbes, *Cryst. Growth Des.*, 2014, *14*, 1357–1365. (e) D. Natale, J. C. Mareque-Rivas, *Chem. Commun*., 2008, 425–437 (f) L. Brammer, *Dalton Trans*., 2003, 3145–3157. (f) L. Meazza,; J. A. Foster, K. Fucke, P. Metrangolo, G. Resnati, J. W. Steed, *Nature Chem.,* 2013, 5, 42-47.
(8) (a) G. Metrangolo, G. Resnati, Halogen Bonding; Fundamentals and Applications , Springer, Berlin, 2008. (b) P. Metrangolo, F. Meyer, T. Pilati, G. Resnati, G. Terraneo, *Angew. Chem., Int. Ed.* 2008, 47, 6114–6121. (c) K. Rissanen, *CrystEngComm*, 2008, 10 1107-1113. (d) G. Metrangolo, G. Resnati, *Cryst. Growth Des.,* 2012, *12*, 5835–5838.
(9) (a) G. Mínguez Espallargas, F. Zordan, L. Arroyo Marín, H. Adams, K. Shankland, J. van de Streek, L. Brammer, *Chem-Eur. J.*, 2009, 15, 7554–7568. (b) F. F. Awwadi, R. D. Willett, B. Twamley, R. Schneider, C. Landee, *Inorg. Chem.* 2008, 47, 9327–9332. (c) F. Zordan, L. Brammer, P. Sherwood, *J. Am. Chem. Soc*., 2005, *127*, 5979–5989. (d) D. A. Smith, L. Brammer, C. A. Hunter, R. N. Perutz, *J. Am. Chem. Soc.*, 2014, 136, 1288–1291 (e) H. R. Khavasi, A. Azhdari Tehrani, *Inorg. Chem.*, 2013, *52,* 2891–2905. (f) K. Akhbari, A. Morsali, *CrystEngComm*, 2012, 14, 1618-1628. (g) F. F. Awwadi, D. Taher, S. F. Haddad, M. M. Turnball, *Cryst. Growth Des.*, 2014, 14, 1961–1971. (h) M. B. Andrews, C. L. Cahill, *Dalton Trans.*, 2012, 41, 3911-3914. (i) K. P. Carter, C. H. F. Zulato, C. L. Cahill, *CrystEngComm*, 2014, 16, 10189-10202 . (j) J. E. Ormond-Prout, P. Smart, L. Brammer, *Cryst. Growth Des.*, 2012, *12,* 205–216. (k) S. Muniappan, S. Lipstmana, I. Goldberg, *Chem. Commun*., 2008, 1777-1779 (l) B. Li, M-M Dong, H-T. Fan, C-Q. Feng, S-Q. Zang, L-Y W., *Cryst. Growth Des*., 2014, 14, 6325–6336 (M) M-M Dong, L-L He, Y-J. Fan, S-Q. Zang, H-W. Hou, T. C. W. Mak, *Cryst. Growth Des*., 2013, 13, 3353–3364.
(10) (a) G. M. Espallargas, L. Brammer, D. R. Allan, C. R. Pulham, N. Robertson, J. E. Warren, *J. Am. Chem. Soc*., 2008, *130*, 9058–9071 (b) G. Metrangolo, G. Resnati, *Chem. Commun.,* 2013, 49, 1783—1785. (c) S-Q. Zang, Y-J. Fan, J-B. Li, H-W. Hou, T. C. W. Mak, *Cryst. Growth Des*. 2011, 11, 3395–3405 (d) M. T. Johnson, Z. Džolić, M. Cetina, O. F. Wendt, L. Öhrström, K. Rissanen, *Cryst. Growth Des.* 2012, 12, 362–368. (e) F. Zordan, L. Brammer, *Acta Cryst*. 2004, B60, 512-519. (f) P. Smart, Á. Bejarano-Villafuerte, L. Brammer, *CrystEngComm*, 2013,15, 3151-3159 (g) P. Smart, Á. Bejarano-Villafuerte, R. M. Hendrya, L. Brammer, *CrystEngComm*, 2013, 15, 3160-3167.
(11) (a) G. Mahmoudi, A. Morsali, *CrystEngComm*, 2009,11, 1868-1879. (b) G. Mahmoudi, A. Morsali, *CrystEngComm*, 2009, 11, 50-51. (c) G. Mahmoudi, A. Morsali, *Cryst. Growth Des.*, 2008, 8, 391–394. (d) A. Morsali, M. Y. Masoomi, *Coord. Chem. Rev*., 2009, 253, 1882-1905. (e) G. Mahmoudi, A. Morsali, *Z. Anorg. Allg. Chem.* 2009, 635, 2697-2700. (f) G. Mahmoudi, A. Morsali, L-G. Zhu, *Z. Anorg. Allg. Chem*. 2007, 633, 539-541. (g) G. Mahmoudi, A. Morsali, *Z. Anorg. Allg. Chem*. 2009, 635, 2697-2700. (h) G. Mahmoudi, A. Morsali, *Inorg. Chim. Acta*, 2008, 362, 3238 (i) M. Y. Masoomi, G. Mahmoudi, A. Morsali, *J. Coord. Chem*., 2010, 63, 1186-1193.
(12) (a) J. J. McKinnon, M. A. Spackman, A. S. Mitchell, *Acta Cryst.,* 2004, B60, 627–668 (b) M. A. Spackman, J. J. McKinnon, *CrystEngComm*, 2002, 4, 378–392.
(13) (a) T. Gelbrich, M. B. Hursthouse, *CrystEngComm,* 2005, 7, 324–336 (b) T. Gelbrich, M. B. Hursthouse, *CrystEngComm,* 2006, 8, 448–460.

(14) F. Macrae, I. J. Bruno, J. A. Chisholm, P. R. Edgington, P. McCabe, E. Pidcock, L. Rodriguez-Monge, R. Taylor, J. van de Streek and P. A. Wood, *J. Appl. Cryst.*, 2008, 41, 466-470.
(15) A. W. Addison, T. N. Rao, J. Reedijk, J. Van Rijn, G. C. Verschoor, *J. Chem. Soc., Dalton Trans.* 1984, 1349–1356.
(16) (a) J. B. King, M. R. Haneline, M. Tsunoda, F. P. Gabbai, *J. Am. Chem. Soc*., 2002, 124, 9350–9351; (b) P. Pyykkö, *Chem. Rev*., 1997, 97, 597–636; (c) J. Y. Wu, H. Y. Hsu, C.-C. Chan, Y.-S. Wen, C. Tsai, *Cryst. Growth Des*., 2009, 9, 258–262.
(17) L. Yang, D. R. Powell, R. P. Houser, *Dalton Trans*. 2007, 955–964.
(18) (a) M. S. Bharara, T. H. Bui, S. Parkin, D. A. Atwood, *Dalton Trans.* 2005, 3874-3880. (b) J. B. King, M. R. Haneline, M. Tsunoda, F. P. Gabbai, *J. Am. Chem. Soc.*, 2002, 124, 9350–9351.
(19) (a) D. Braga, *J. Chem. Soc*., *Dalton Trans*., 2000, 3705–3713 (b) L. Brammer, *Chem. Soc. Rev.*, 2004, 33, 476–489. (c) E. R. T. Tiekink, *Chem. Commun.*, 2014, 50, 11079-11082. (d) E. Constable, G. Zhang, C. E. Housecroft, J. A. Zampese, *CrystEngComm*, 2011, 13, 6864-6870.
(20) (a) C. S. Lai, S. Liu, E. R. T. Tiekink, *CrystEngComm*, 2004, 6, 221–226. (b) I. Beletskaya, V. S. Tyurin, A. Y. Tsivadze, R. Guilard, C. Stern, *Chem. Rev.*, 2009, 109, 1659–1713. (c) H. R. Khavasi, A. R. Salimi, H. Eshtiagh-Hosseini, M. M. Amini, *CrystEngComm*, 2011, 13, 3710-3717. (d) H. R. Khavasi, B. Mir Mohammad Sadegh, *Dalton Trans.*, 2014, 43, 5564-5573 (e) C. Bazzicalupi, A. Bianchi, E. Garcia-Espaňa, E. Delgado-Pinar, *Inorg. Chim. Acta.,* 2014, 417, 3-26. (f) H. S. Jena, *New J. Chem.*, 2014, 38, 2486-2499. (g) S. K. Chandran, R. Thakuria, A. Nangia, *CrystEngComm*, 2008, 10, 1891-1898.
(21) S. P. Ananthavel, M. Manoharan, *Chem. Phys*. 2001, 269, 49–57.
(22) (a) P. Politzer, J. S. Murray, T. Clark, *Phys. Chem. Chem. Phys*. 2010, 12, 7748–7757. (b) P. Metrangolo, H. Neukirch, T. Pilati, G. Resnati, *Acc. Chem. Res.* 2005, 38, 386–395. (c) J. S. Murray, K. E. Riley, P. Politzer, T. Clark, *Aust. J. Chem.* 2010, 63, 1598–1607.
(23) (a) G. Cavallo, P. Metrangolo, T. Pilati, G. Resnati, G. Terraneo, *Cryst. Growth Des.*, 2014, 14, 2697–2702. (b) C. B. Aakeröy, M. Fasulo, N. Schultheiss, J. Desper, C. Moore, *J. Am. Chem. Soc.*, 2007, *129*, 13772–13773 (c) C. B. Aakeröy, P. D. Chopade, J. Desper, *Cryst. Growth Des*., 2013, 13, 4145-4150. (d) H. R. Khavasi, M. Hosseini, A. Azhdari Tehrani, S. Naderi, *CrystEngComm*, 2014, 16, 4546-4553 (e) H. R. Khavasi, A. Ghanbarpour, A. Azhdari Tehrani, *CrystEngComm*, 2014, 16, 749-752 (f) P. Metrangolo, G. Resnati, *Cryst. Growth Des.*, 2012, 12, 5835–5838. (g) N. Han, Y. Zeng, C. Sun, X. Li, Z. Sun, L. Meng, *J. Phys. Chem. A*, 2014, 118, 7058–7065
(24) R. Bertani, P. Sgarbossa, A.Venzo, F. Lelj, M. Amati, G. Resnati, T. Pilati, P. Metrangolo, G. Terraneo, *Coord. Chem. Rev*. 2010, 254, 677–695.
(25) L. Brammer, G. M. Espallargas, S. Libri, *CrystEngComm*, 2008, 10, 1712-1727.
(26) J. D. H. Donnay, D. Harker, *Am. Mineral*., 1937, 22, 446-467.
(27) Agilent Technologies (2010). CrysAlis PRO Version 1.171.35.15 (release 03–08–2011 CrysAlis171.NET).
(28) L. J. Farrugia, *J. Appl. Crystallogr.,* 1999, 32, 837–838.
(29) C. Altomare, G. Cascarano, C. Giacovazzo, A. Guagliardi, *J. Appl. Crystallogr.*, 1993, 26, 343–350.
(30) G. M. Sheldrick, *Acta Crystallogr., Sect. A: Found. Crystallogr.,* 2008, 64, 112–122.
(31) F. Neese, U. Becker, D. Ganyushin, D. G. Liakos, S. Kossmann, T. Petrenko, C. Riplinger, F. Wennmohs, ORCA, 2.7.0, University of Bonn, Bonn, 2009.
(32) (a) A. D. Becke, *Phys. Rev*., 1988, 38, 3098-3100 (b) C. Lee, W. Yang, R. G. Parr, *Phys. Rev. B: Condens. Matter Mater. Phys*., 1988, 37, 785-789.
(33) S. Grimme, J. Antony, S. Ehrlich, H. Krieg, *J. Chem. Phys*., 2010, 132, 154104-154119.
(34) C. Fonseca Guerra, H. Zijlstra, G. Paragi, M. Bickelhaupt, *Chem – Eur. J*., 2011, 17, 12612-12622.
(35) (a) E. van Lenthe, E. J. Baerends, J. G. Snijders, *J. Chem. Phys*., 1993, 99, 4597–4610 (b) E. van Lenthe, E. J. Baerends, J. G. Snijders, *J. Chem. Phys.*, 1994, 101, 9783–9792; (c) E. van Lenthe, van R. Leeuwen, E. J. Baerends, J. G. Snijders, *Int. J. Quantum Chem*., 1996, 57, 281–293.

Graphical Abstract